

Metallacycles

Condensed Osmquinolines with NIR-II Absorption Synthesized by Aryl C–H Annulation and Aromatization

Fei-Hu Cui, Qian Li, Le-Han Gao, Kaidong Ruan, Kexin Ma, Siyuan Chen, Zhengyu Lu, Jiawei Fei, Yu-Mei Lin,* and Haiping Xia*

How to cite: *Angew. Chem. Int. Ed.* **2022**, *61*, e202211734

International Edition: doi.org/10.1002/anie.202211734

German Edition: doi.org/10.1002/ange.202211734

Abstract: The structural design and tuning of properties of metallaaromatics are crucial in materials and energy science. Herein, we describe the rapid synthesis of tetracyclic metallaaromatics containing quinoline and pentalene motifs fused by a metal-bridged fragment. These unique compounds display remarkably broad absorption, enabling for the first time the absorption of metallaaromatics to reach the second near-infrared (NIR-II) bio-window. The formation of osmaquinoline unit involves an unconventional C(sp²)–C(sp³) coupling promoted by AgBF₄ to achieve [3+3] cycloaddition. The introduction of cyclic d_π–p_π conjugation and extension of the aromatic π-framework can effectively shrink the HOMO–LUMO gap, thus broadening the absorption window. The considerable photothermal conversion efficiency (PCE) in both the NIR-I and NIR-II windows, the high photothermal stability and the excellent electrochemical behavior suggest many potential applications of these condensed metallaquinolines.

Introduction

Aromatic compounds enjoy many applications in pharmaceutical and material sciences.^[1] Formal replacement of one CH group in aromatic molecules by an isolobal transition-metal fragment leads to metallaaromatics, which have recently been attracting increasing attention.^[2] The introduction of d_π–p_π conjugation involving the overlap of the transition metal d orbitals. These promote many applications, such as synthesis of conjugated polymers,^[3] photoactive therapy of hypoxic tumors^[4] and solar cells.^[5] Some metallaaromatics display the first near-infrared absorption (NIR-I, 700–1000 nm), making them promising photothermal agents (PTA).^[6] Materials with second near-infrared

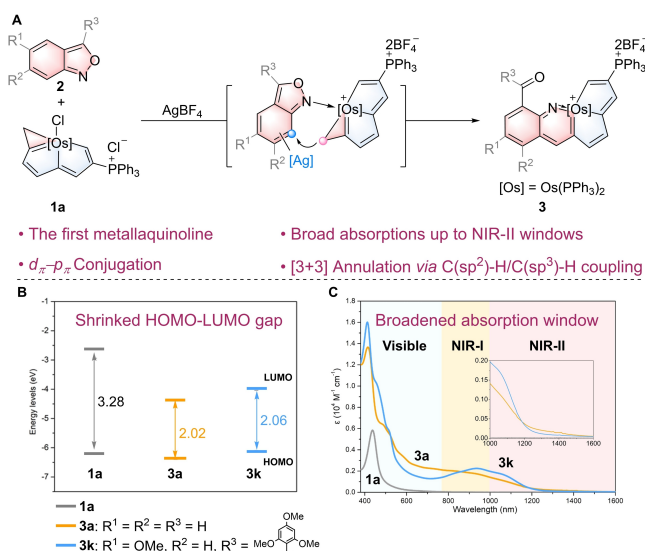
(NIR-II, 1000–1700 nm) absorbing ability are significant in photothermal therapy as a result of their minimized phototoxicity and deeper tissue penetration.^[7] To date, the reported NIR-II absorbing molecules include a few inorganic materials,^[8] conjugated polymer nanoparticles (NPs),^[9] supramolecular radicals,^[10] and organic molecules with complex structures.^[11] It is desirable to rationally design new species and thus expand the library of NIR-II absorbing materials. Metallaaromatics that involve transition metals usually have HOMO–LUMO gaps that are narrower than those of their organic counterparts.^[3] Rational design of metallaaromatics by extending their π-conjugation and/or modulating the electronic effects of substituents could be a feasible strategy with which to broaden the absorption to the NIR-II window.

N-heteroarenes are important because of their wide applications in the pharmaceutical industry, materials science, catalysis and organometallic chemistry.^[12] Condensed N-containing aromatics are commonly used to modulate the band gap of materials.^[13] Anthranil is a significant aromatic heterocycle and can serve as a building block that potentially could extend π-conjugation.^[14] Anthranil derivatives with diverse substituents are readily accessible,^[15] thus it is feasible to install various groups in anthranils to modulate the strength of the charge transfer. These characteristics have encouraged us to explore the reaction of anthranils with metallaaromatics with the aim of discovering new π-extended aza-metallaaromatics with broad absorptions.

Here we present a new [3+3] annulation method for rapid construction of an osmaquinoline ring by the reaction of anthranil with osmacyclopropene (Scheme 1A). This reaction involves an unconventional C(sp²)–C(sp³) coupling enabled by the synergistic effects of the Ag and Os metals. The role of AgBF₄ in promotion of aryl C–H annulation was confirmed by the isolation of a key Ag-anthranil intermediate. The tetracyclic metallaaromatics that are obtained contain quinoline and pentalene motifs fused by a metal-bridged fragment. The extending aromatic π-framework can effectively shrink the HOMO–LUMO gap (3.28 eV for **1a** vs 2.02 eV for **3a**, Scheme 1B) thus broadening the absorption window, and enabling the products to exhibit remarkably broad absorptions spanning from UV/Visible to the NIR-I and NIR-II windows (up to 1400 nm, Scheme 1C). The condensed osmaquinolines show considerable photothermal conversion efficiency at both the NIR-I and NIR-II windows, in addition to high photothermal stability. This work describes an unusual reactivity pattern of anthranil,

[*] F.-H. Cui, Q. Li, L.-H. Gao, K. Ruan, K. Ma, S. Chen, J. Fei, Prof. Y.-M. Lin, Prof. H. Xia
 College of Chemistry and Chemical Engineering
 Xiamen University
 Xiamen 361005 (China)
 E-mail: linyum@xmu.edu.cn
 hpxia@xmu.edu.cn

Dr. Z. Lu, Prof. H. Xia
 Shenzhen Grubbs Institute, Department of Chemistry
 Southern University of Science and Technology
 Shenzhen 518055 (China)



Scheme 1. A) Facile synthesis of condensed osmaquinolines (**3**) through C–H annulation of anthranil (**2**) with cyclopropa-osmapentalene (**1a**). B) The HOMO–LUMO gaps. C) Absorption spectra of cyclopropa-osmapentalene (**1a**) and condensed osmaquinolines (**3a**, **3k**).

and provides a new strategy for synthesis of intriguing polycyclic π -systems.

Results and Discussion

Aromatic cyclopropa-osmapentalene (**1a**) contains a strained metallacyclopentene moiety.^[21] On the other hand, anthranil is a significant aromatic heterocycle that can be converted into organic N-heterocycles through various reaction modes.^[16] Because anthranil can coordinate through nitrogen to metals and the N–O bond is polarized and cleavable, it was thought to be interesting to investigate the reactions between them. Treatment of cyclopropa-osmapentalene (**1a**) and anthranil (**2a**) with AgBF_4 at 40 °C in CH_2Cl_2 for 6 h led to the formation of a complex (**3a**) with an isolated yield of 90 % (Figure 1A). The initial purpose of addition of the silver salt into the reaction system is dissociating the chlorine ligand and promoting the coordination of anthranil to osmium center. The reaction proceeds through a formal [3+3] cycloaddition of the metallacyclopentene unit with anthranil to construct an osmaquinoline motif, leading to the formation of a ring-expanded and ring-annulated product, a unique condensed metallaquinoxaline. To investigate the scope and generality of this reaction, cyclopropa-osmapentalenes (**1a–b**) and substituted anthranils (**2a–j**) were examined and generated the corresponding condensed metallaquinoxalines **3a–k** in 81–91 % yields (see the details in S6 of Supporting Information).

All the compounds that have been synthesized were characterized by nuclear magnetic resonance spectroscopy (NMR), high-resolution mass spectrometry (HRMS), and the structures of complexes **3c**, **3g**, **3h**, **3j**, and **3k** were further confirmed by X-ray crystallographic analysis.^[17] The

single-crystal structure of complex **3c** confirmed the formation of a ring-expansion product from the parent metallacyclopentene unit (Figure 1B and Figure S1 in the Supporting Information). The skeleton of **3c** contains a metallaquinoxaline moiety fused with a metallapentalene. The osmium center in **3c** is six-coordinated with an octahedral coordination geometry. The metal center is positioned at the ring junction of the fused five-membered rings and a six-membered pyridine ring. The equatorial polycyclic ring system (composed of Os1, N1, and C1–C14) is almost coplanar, as reflected by the mean deviation of the least-squares plane (0.085 Å). The nearly equal Os–C bond lengths (Os1–C1 2.053(2) Å, Os1–C4 2.125(2) Å, and Os1–C7 2.063(2) Å) indicate a delocalized structure. The bond lengths of Os1–N1 (1.847(18) Å) and N1–C10 (1.288(3) Å) suggest the cumulated double bonds, whose lengths are close to those of reported osmapyridyne (1.891(3) and 1.270(5) Å).^[18] The bond length of O1–C15 (1.206(3) Å) indicates an aldehyde group attached to C11. The C–C bond lengths (1.363(4)–1.470(3) Å) in the tetracyclic system are between the lengths of C–C single and double bonds and show no significant bond-length alternation. The planarity and the bond lengths indicate a delocalized metallatetracyclic compound. The structural parameters (bond lengths and bond angles) of complexes **3g**, **3h**, **3j**, and **3k** are comparable with those of complex **3c** (Figure 1B and S14 in the Supporting Information).

Together with the results of X-ray diffraction, the ¹H NMR signal of the proton on the C1(H1) in **3c** (S8 in the Supporting Information) is observed at $\delta = 13.67$ ppm. Other proton signals on the fused five-membered rings are found in the aromatic region, $\delta = 8.97$ (H3), 9.48 (H5), and 8.41 (H6) ppm, respectively. The proton signal of aldehyde group is observed at $\delta = 9.73$ (H15) ppm. In the ¹³C NMR spectrum, the signals of metal-bonded C1 (232.9 ppm), C7 (206.0 ppm) and C4 (196.9 ppm) are consistent with partial double bond character for these bonds. The ³¹P NMR spectrum shows two singlets at 16.82 (C₃PPh₃) and –5.49 ppm (OsPPh₃). The HRMS displays a prominent molecular ion at $m/z = 613.6512$ with the expected isotopic distribution (calculated value [C₇₀H₅₂NO₂OsP₃]²⁺ at $m/z = 613.6564$).

In view of the structural features of complexes **3a–3k**, they can be recognized as a quinoxaline and a pentalene fused by a metal-bridged fragment. Such a fused skeleton is inaccessible by only two organic frameworks, as the bridge-head transition-metal atom could provide larger coordination numbers than a bridge-head carbon atom. Incorporation of nitrogen or metal into π -conjugated systems can significantly modify the chemical and physical properties.^[21,13,19] N-containing metallaaromatics such as metallapyridine,^[20] metallaisoxazole,^[21] and metallaisoquinoline derivatives^[22] have been synthesized. The title compounds are the new π -extended aza-metallaaromatics containing metallaquinoxalines.

We conducted a series of control experiments with the aim of clarifying the mechanism of this reaction. First, the stoichiometric reaction of AgBF_4 with complex **1a** in CH_3CN led to removal of the chloride ligand through

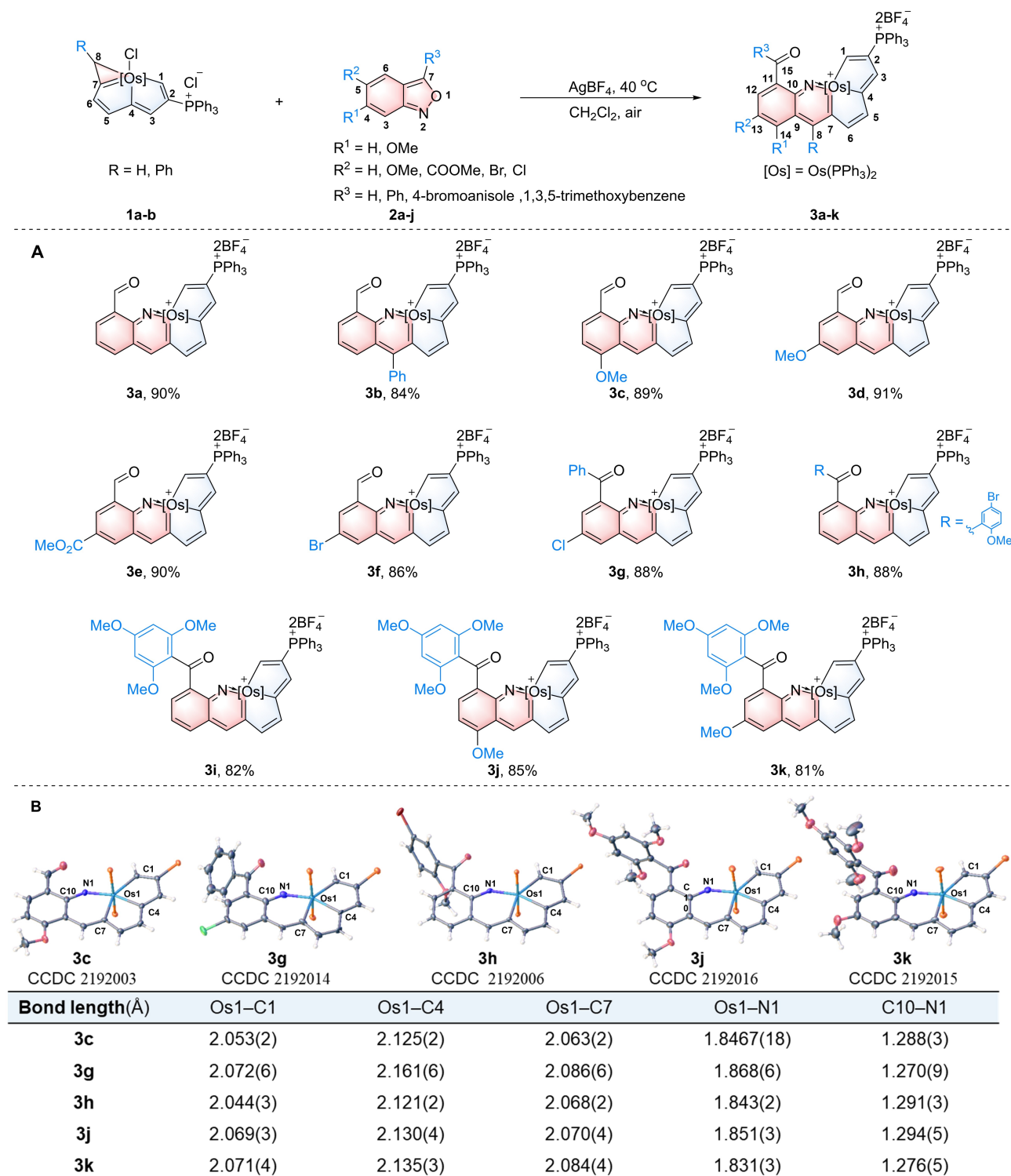


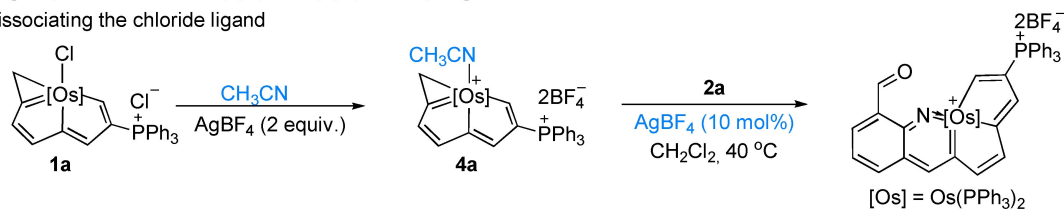
Figure 1. A) Reaction scope of cycloprosa-osmapentalene (**1**) and anthranil (**2**). B) X-ray structures for **3c**, **3g**, **3h**, **3j**, and **3k** drawn with 50% probability level. The phenyl groups in PPh₃ have been omitted for clarity. Selected bond lengths (Å) in **3c**, **3g**, **3h**, **3j**, and **3k**.

precipitation as silver chloride and replacement by CH₃CN and formation of **4a** (Figure 2A, i). The isolated species (**4a**) was employed in the model reaction with a catalytic amount AgBF₄ (10 mol %), leading to the corresponding product (**3a**) in comparable (90%) yield. Remarkably, a silver-

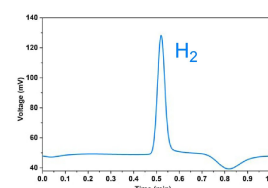
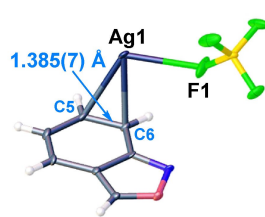
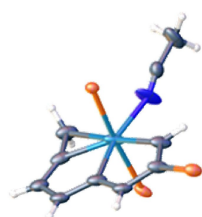
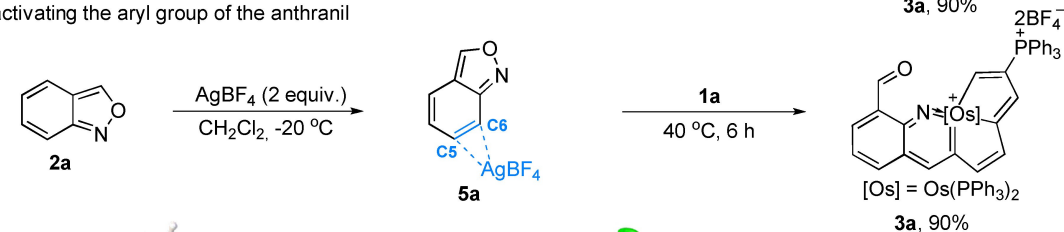
anthranil adduct (**5a**) was identified by an in situ crystallization experiment at –20 °C (Figure 2A, ii). The single-crystal structure of **5a** revealed the interaction of AgBF₄ with anthranil. The distances of Ag1–C6 (2.364(5) Å) and Ag1–C5 (2.532(6) Å) suggest that the p_π-coordination of

A. AgBF_4 facilitates the $\text{C}(\text{sp}^3)\text{-H}/\text{C}(\text{sp}^2)\text{-H}$ coupling

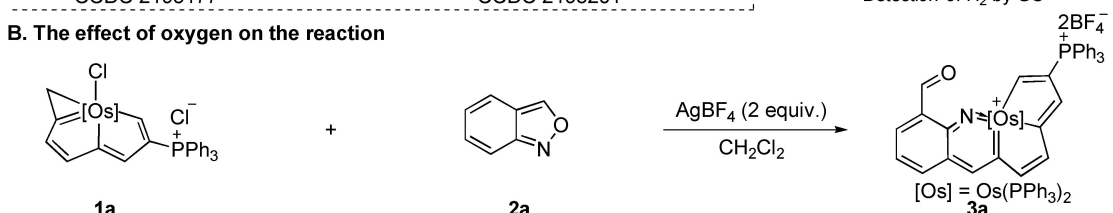
(i) dissociating the chloride ligand



(ii) activating the aryl group of the anthranil



B. The effect of oxygen on the reaction



Entry	Conditions	Yield of 3a	Detection of H ₂ by GC
1	Nitrogen	89%	Detected
2	Oxygen	90%	Trace
3	Air	90%	Trace

C. Plausible mechanism for the formation of complex 3a in air atmosphere

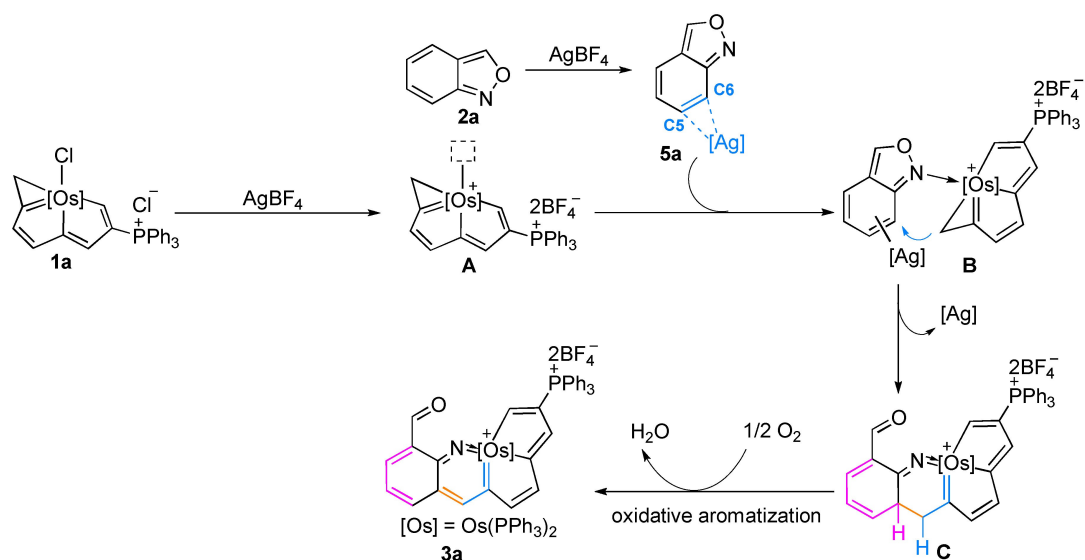


Figure 2. A) AgBF_4 facilitates the $\text{C}(\text{sp}^3)\text{-H}/\text{C}(\text{sp}^2)\text{-H}$ coupling: (i) dissociation of the chloride ligand by AgBF_4 and catalytic amount of AgBF_4 (10%) triggering the effective [3+3] annulation reaction starting from 4a; (ii) identifying the AgBF_4 and anthranil interaction species 5a; B) The effect of oxygen on the reaction. C) Plausible mechanism for the formation of complex 3a.

Ag^+ to anthranil and thus make C_6 electrophilic. Consistently, the bond length of C3–C4 (1.385(7) Å) is longer than the typical aryl C–C bond (Figure S7 in the Supporting Information). Further studies showed that addition of **1a** into the pre-prepared silver-anthranil adduct (**5a**) delivered the product (**3a**) in 90 % yield. These results suggest that the silver salt facilitates the subsequent $\text{C}(\text{sp}^3)\text{--H}/\text{C}(\text{sp}^2)\text{--H}$ coupling.

Next, we examined the effect of oxygen on the reaction. As shown in Figure 2B, reaction of **1a** with **2a** can proceed smoothly in either oxygen atmosphere or nitrogen atmosphere. A clear hydrogen signal can be detected by gas chromatography (GC) analysis in a nitrogen atmosphere, whereas in an oxygen atmosphere almost no hydrogen is formed in the reaction mixture. On the basis of these experimental results and previous reports, we speculate that the formation of **3a** may undergo different aromatization pathways in nitrogen or oxygen atmospheres, namely spontaneous aromatization^[23] accompanied by hydrogen generation or oxygen-promoted oxidative aromatization,^[24] respectively (S14 in the Supporting Information).

Based on these experiments and the reactivity of the metallacyclopropene (**1**) with alkenes or alkynes,^[25] a plausible mechanism for the formation of **3a** in air (O_2) atmosphere is proposed (Figure 2C). Initially, removal of the Cl ligand in **1a** by AgBF_4 gave the intermediate (**A**) with a vacant metal center. At the same time, AgBF_4 activates the aryl C–C bond of anthranil to give an adduct **5a**. This is followed by coordination of **5a** and **A**, affording the intermediate (**B**). Next, N–O bond cleavage occurs and is followed by intramolecular C–C coupling, generating an annulation species (**C**). Subsequently, the final product **3a** was generated via a process of oxygen-promoted oxidative aromatization.^[24c,d]

The above results concerning the mechanism reveal that the silver salt plays an important role in the transformation by dissociating the chloride ligand of **1a** and activating the aryl group of the anthranil. In addition, the active $\text{C}(\text{sp}^3)\text{--H}$ in an osmacyclopropene unit and the coordination of anthranil to Os center directing the reaction components into close proximity are also beneficial to the $\text{C}(\text{sp}^3)\text{--H}/\text{C}(\text{sp}^2)\text{--H}$ cross-coupling. In this regard, the unique [3+3] annulation of anthranil with osmacyclopropene is promoted by the synergistic effects of the Ag and Os metals.

The activation by silver of the aryl C–C of anthranil observed in this reaction is unique. Anthranils usually serve as nucleophiles which attack with either their nitrogen atom or oxygen atom, enabling access to a variety of N-heterocycles with various degrees of molecular complexity.^[26] Compared with the highly reactive isoxazole moiety, aryl C–H annulation of anthranils has rarely been reported. Hashmi et al. described a gold-catalyzed *ortho*-aryl C–H annulation of anthranil to afford 7-acylindoles.^[14a,26a] Wu et al. recently reported a copper-catalyzed oxidative cross-coupling reaction for site-selective C5-dicarbonylation reaction of anthranils.^[27] These examples rely on *o*-imino gold carbenes or phenyl glyoxal as key electrophilic intermediates. The unusual activation of the C3–H site of anthranil by

a silver salt, generating a silver-anthranil adduct has not been reported previously.

The observed downfield NMR signals, delocalized bond lengths, and planarity of the tetracyclic framework suggest the aromaticity of compounds **3a–3k**. We further calculated the nucleus-independent chemical shift (NICS) values based on the model compound **3k'** in which the PPh_3 ligands are replaced by PH_3 groups. In general, negative NICS values indicate aromaticity and the calculated NICS values for complex **3k'** of rings A, B, C, and D are –25.8, –13.9, –14.7, and –7.9 ppm, respectively, suggesting the aromatic character of **3k'** (Figure 3A). The aromaticity of **3k'** is further supported by anisotropy of the induced current density (AICD) analysis. As shown in Figure 3A and Figure S8 in Supporting Information, the current density vectors plotted on the AICD isosurface indicate a clockwise ring current. The calculation results are in good agreement with the experimental results, indicating that the tetracyclic complex **3k** is aromatic.

The stability in the solid state of selected complexes **3** have been examined by heating in air for 3 h. Complexes **3a**, **3e**, **3g**, **3h**, **3j**, and **3k** are all stable under 140 °C (Figure 3B). Complex **3e** with electron-withdrawing group ($-\text{COOMe}$) begins to decompose at 160 °C, while those with strong electron-donating groups **3j** and **3k** are more stable and can survive at 180 °C. As monitored by UV/Vis-NIR spectroscopy, no decomposition was observed after the dichloromethane solution of **3k** had been stored under ambient conditions for twenty days (Figure 3C). The robust properties of these metallatetracyclic compounds in both the solid and solution state are significant for their future applications.

The UV/Vis-NIR absorption spectra showed that these condensed metallaaromatics exhibit broad absorption bands

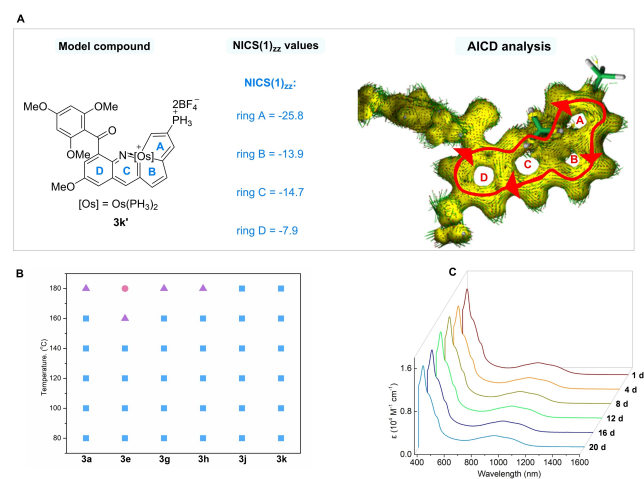


Figure 3. A) Aromaticity evaluations. NICS(1)_{zz} values (in ppm) of **3k'** calculated at the B3LYP/6-31G* level. The isosurface value of the AICD plots is 0.030 a.u. The magnetic field vector is orthogonal with respect to the ring plane and is directed upwards (clockwise currents are diatropic). B) Thermal stabilities of **3a**, **3e**, **3g**, **3h**, **3j**, and **3k** in the solid state, all reactions were carried out for 3 hours in air, ■ = stable, ▲ = partly decomposed, ● = completely decomposed. C) Stability of **3k** in solution in CH_2Cl_2 in an air atmosphere.

ranging from the ultraviolet to the visible region and extending to the near-infrared region. As shown in Figure 4B, the precursor **1a** displays an absorption maximum at 437 nm with molar absorption coefficient value (ϵ) of $5940 \text{ M}^{-1} \text{ cm}^{-1}$. In contrast, the π -extended tetracyclic complexes (**3**) show remarkably strong and broad absorption bands reaching the near-infrared regions (NIR-I and NIR-II).

II). For example, complex **3k** shows considerable strong absorption at 413 nm with molar absorption coefficient value (ϵ) of $17147 \text{ M}^{-1} \text{ cm}^{-1}$ and an absorption band can be spanned to 1400 nm. The NIR absorption intensity can be tuned by changing the substituents (Figures 4A, 4B). The 2, 4, 6-trimethoxybenzaldehyde-substituted osmaquinoline-fused metallaromatic (**3i**) for example, exhibits strong

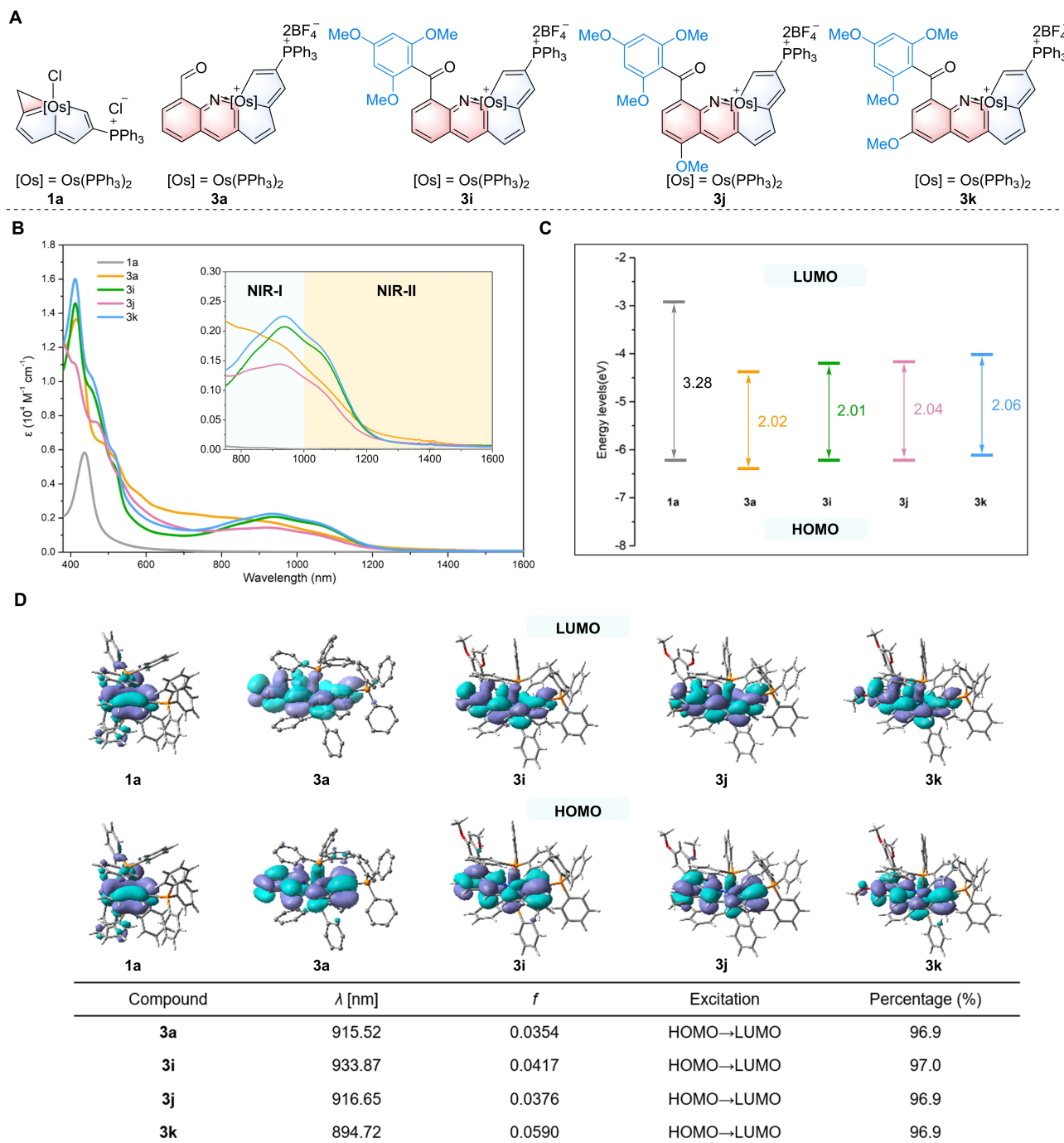


Figure 4. A) Structures of **1a**, **3a**, **3i**, **3j**, and **3k**. B) UV/Vis-NIR absorption spectra of **1a**, **3a**, **3i**, **3j**, and **3k** measured in CH_2Cl_2 at room temperature. C) Calculated HOMO and LUMO energy levels. D) DFT calculated lowest unoccupied molecular orbitals (LUMO), the highest occupied molecular orbitals (HOMO) for the cations of **1a**, **3a**, **3i**, **3j**, and **3k**, excited wavelength, (λ) oscillator strengths (f) and related wavefunctions.

absorption in the NIR-I window with a molar absorption coefficient value (ϵ) of $3084 \text{ M}^{-1} \text{ cm}^{-1}$ at 808 nm. Introduction of a methoxy group to C13 of the aromatic framework (**3k**) leads to the increased absorption at 925 nm ($\epsilon = 2560 \text{ M}^{-1} \text{ cm}^{-1}$). Such an effect is reduced when methoxy group was shifted to C14 of the aromatic framework (**3j**).

To further study the absorption spectra of these π -conjugated tetracyclic metallaromatics, time-dependent density functional theory (TD-DFT) calculations were carried out at the B3LYP/6-31G(d) level. The results show that energy level of the highest occupied molecular orbitals (HOMO) of **1a**, **3a**, **3i**, **3j**, and **3k** are nearly identical, but the energy level of the lowest unoccupied molecular orbital (LUMO) of **1a** is obviously higher than that of **3a**, **3i**, **3j**, and **3k** (Figure 4C). This feature favors narrowing the HOMO–LUMO gap, and because of this, the red-shifted absorption bands of **3a**, **3i**, **3j**, and **3k** in comparison with that of **1a** can be rationalized.

The HOMOs and LUMOs of these compounds are mainly delocalized on the osmaquinoline skeletons and the absorption bands in the near-infrared region contribute mainly to the local excitation (LE) from HOMO to LUMO (Figure 4D). The calculated excited wavelength (λ) and the corresponding oscillator strengths (f) of **3a** (916 nm, $f = 0.0354$), **3i** (934 nm, $f = 0.0417$), **3j** (917 nm, $f = 0.0376$), and **3k** (895 nm, $f = 0.0590$) are in good agreement with the

experimental observations concerning the intensity of absorption spectra (Figure 4D).

The common strategies for extending absorption to the NIR-II window involve incorporation of conjugated cyclic moieties or modulation of donor and acceptor units (D–A effect), leading to complex organic molecules or large conjugated polymers.^[9,11] In this work, as transition metals usually have narrow HOMO–LUMO gaps,^[3] a cyclic $d_{\pi}p_{\pi}$ conjugation strategy involving the overlap of the transition metal d orbitals has been demonstrated for extending the absorption, and the metallaromatics with NIR-II absorbing ability were realized for the first time. The findings provide a new perspective for the design of NIR-II absorbing molecules.

Because of the broad absorbance spectra, the photothermal properties of these metallaromatics (**3a**, **3i**, **3j**, and **3k**) in the NIR-II region were examined under 1060 nm laser irradiation. As shown in Figure 5A, the temperatures of **3a**, **3i**, **3j**, and **3k** solutions all increased under 1060 nm laser irradiation and the temperature of **3k** rises faster than the others. Under the same conditions (1060 nm, 1 W cm^{-2}), the temperature of **3k** solution increased from 27.1 to $86.3 \text{ }^{\circ}\text{C}$ ($\Delta T = 59.2 \text{ }^{\circ}\text{C}$), which is more than that of **3a**, which goes from 26.8 to $82.7 \text{ }^{\circ}\text{C}$ ($\Delta T = 55.9 \text{ }^{\circ}\text{C}$). The pure solvent shows a negligible temperature change under similar conditions and the corresponding infrared images are shown in Figure 5B. According to the change in the temperature, the

Photothermal properties under 1060 nm laser irradiation

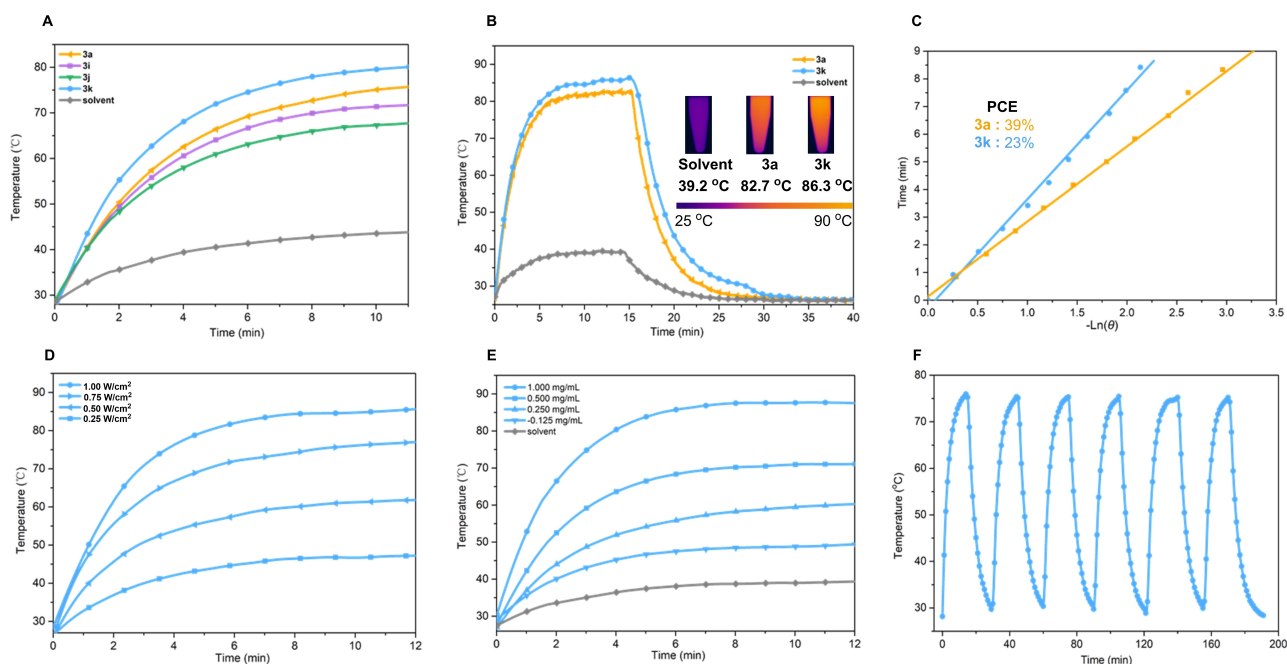


Figure 5. A) Photothermal conversion of **3a**, **3i**, **3j**, and **3k** (0.500 mg mL^{-1}) under 1060 nm (4.00 W cm^{-2}) laser irradiation. B) Photothermic heating curves of **3a** and **3k** (1.000 mg mL^{-1}) under 1060 nm (1.00 W cm^{-2}) laser irradiation for 15 min followed by cooling to room temperature and infrared imaging of **3a** and **3k**. C) Linear correlation of the cooling times versus negative natural logarithm of driving force temperatures and PCEs. D) Photothermal conversion of **3k** (1.000 mg mL^{-1}) under 1064 nm laser irradiation with different exposure intensity ($0.25\text{--}1.00 \text{ W cm}^{-2}$). E) Photothermal conversion of **3k** at different concentrations ($0.125\text{--}1.000 \text{ mg mL}^{-1}$) under 1064 nm (1.00 W cm^{-2}) laser irradiation. F) Photothermal stability of **3k** (0.500 mg mL^{-1}) upon 1064 nm (4.00 W cm^{-2}) laser irradiation for six on/off cycles.

PCE values of **3a** and **3k** were calculated to be 39 and 23 %, respectively (Figure 5C). Further investigation showed that the temperature elevation profiles of **3k** are positively related to the concentration, as well as the laser power density, revealing the controllable photothermal behavior (Figures 5D, 5E). To investigate the photostability of complex **3k** further, we performed six heating and cooling cycles under 1060 nm laser irradiation and observed no obvious degradation, revealing excellent thermal- and photostability (Figure 5F).

The photothermal conversion abilities of **3a**, **3i**, **3j**, and **3k** were also investigated under 808 nm and 980 nm NIR laser irradiation (Figure S10 in Supporting Information). Under 808 nm laser irradiation, the PCE values of **3a** and **3k** were calculated to be 64 % and 68 %, respectively (Figure S10C and Table S7 in Supporting Information). The PCE values are more than twice those of the previously reported NIR-I absorbing metallaaromatics (26.6 %).^[28] While under 980 nm laser light irradiation (1 W cm⁻²), solutions of **3a** and **3k** rapidly increased in temperature from 27.2 °C to 93.2 °C ($\Delta T=66^\circ\text{C}$), and 27.5 °C to 98.0 °C ($\Delta T=70.5^\circ\text{C}$), respectively (Figure S10E). The PCE of **3a** and **3k** were calculated to be 43 % and 44 %, respectively (Figure S10F and Table S8 in Supporting Information).

We further examined the electrochemical properties of these tetracyclic metallaaromatics. As shown in Figure 6, **3a**, **3d**, **3e**, and **3k** showed a reversible oxidation couplet at half-wave potentials ($E_{1/2}$) of 0.21, 0.10, 0.37, and 0.01 V, respectively. The substituents in the metallaromatic influenced the oxidation and reduction potentials. For example, the introduction of electron-donating groups in complexes **3d** (-OMe) and **3k** (-OMe and 1,3,5-trimethoxybenzene), respectively, caused a cathodic shift in the reduction potential compared with that in **3a**, while the electron-withdrawing group (-COOMe) in complex **3e** led to an anodic shift, relative to that in **3a**. As presented in Table S5 in Supporting Information, the calculated HOMO and LUMO levels also matched well with the changing oxidation

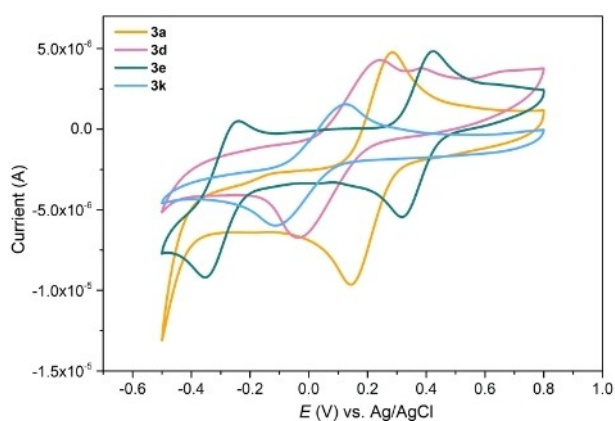


Figure 6. Cyclic voltammograms of **3a**, **3d**, **3e**, and **3k** in CH₂Cl₂ obtained by the cyclic voltammetry (CV) with a glassy carbon as the working electrode, a platinum rod as the auxiliary electrode, Ag/AgCl as the reference electrode, [Bu₄N]PF₆ as the supporting electrolyte and a ferrocene/ferrocenium couple as the external standard.

and reduction potentials. Introduction of electron-donating groups increased both the HOMO and LUMO levels, while electron-withdrawing units caused the opposite result. In this regard, the high stability, low LUMO levels, and reversible oxidation couple of these fused metallaaromatics make them promising candidates for use as electron-acceptors in organic solar cells.^[29]

Conclusion

A [3+3] annulation reaction between anthranil and metallacyclopentene based on a cyclic π -conjugation extending strategy has been developed. The reaction involved activating the aryl fragment of anthranil by AgBF₄, followed by C(sp²)-C(sp³) coupling, leading to the formation of new tetracyclic metallaaromatics containing metallaquinoxaline motifs, which represent an important supplement to the library of rare metal-bridged N-containing metallaaromatics. These conjugated condensed metallacycles exhibit extremely broad absorption extending to the NIR bio-windows, and are new NIR-II absorbing agents. Their good photothermal properties (under 808, 980 and 1060 nm laser irradiations) and excellent reversible electrochemical behavior suggest their potential applications in photoelectric materials, biomedicine and solar energy utilization. Our strategy features a novel reactivity pattern of anthranil for the C-H annulation and opens an avenue for the synthesis of new N-doped condensed metallacycles with intriguing properties.

Acknowledgements

This work is supported by the Natural Science Foundation of China (Nos. 22071206, 92156021 and 21931002), the Natural Science Foundation of Fujian Province of China (No. 2020J01025), the Shenzhen Science and Technology Innovation Committee (no. JCYJ20200109140812302), and the Guangdong Provincial Key Laboratory of Catalysis (no. 2020B121201002).

Conflict of Interest

The authors declare no conflict of interest.

Data Availability Statement

The data that support the findings of this study are available in the supplementary material of this article.

Keywords: Anthranil · $d_{\pi-p_{\pi}}$ Conjugation · Metallaaromatics · NIR-II Absorption · [3+3] Annulation

[1] M. M. Boorum, L. T. Scott, *Modern Arene Chemistry*, Wiley-VCH, Weinheim, 2002.

- [2] a) J. B. Chen, V. G. Young, R. J. Angelici, *J. Am. Chem. Soc.* **1995**, *117*, 6362–6363; b) J. R. Bleeker, *Chem. Rev.* **2001**, *101*, 1205–1227; c) M. Paneque, C. M. Posadas, M. L. Poveda, N. Rendón, V. Salazar, E. Oñate, K. Mereiter, *J. Am. Chem. Soc.* **2003**, *125*, 9898–9899; d) C. W. Landorf, M. M. Haley, *Angew. Chem. Int. Ed.* **2006**, *45*, 3914–3936; *Angew. Chem.* **2006**, *118*, 4018–4040; e) G. Jia, *Coord. Chem. Rev.* **2007**, *251*, 2167–2187; f) M. Saito, M. Sakaguchi, T. Tajima, K. Ishimura, S. Nagase, M. Hada, *Science* **2010**, *328*, 339–342; g) B. J. Frogley, L. J. Wright, *Coord. Chem. Rev.* **2014**, *270*, 151–166; h) J. Wei, Y. Zhang, Y. Chi, L. Liu, W.-X. Zhang, Z. Xi, *J. Am. Chem. Soc.* **2016**, *138*, 60–63; i) M. Batuecas, R. Castro-Rodrigo, M. A. Esteruelas, C. García-Yebra, A. M. López, E. Oñate, *Angew. Chem. Int. Ed.* **2016**, *55*, 13749–13753; *Angew. Chem.* **2016**, *128*, 13953–13957; j) W. Ma, C. Yu, T. Chen, L. Xu, W.-X. Zhang, Z. Xi, *Chem. Soc. Rev.* **2017**, *46*, 1160–1192; k) Y. Zhang, J. Wei, Y. Chi, X. Zhang, W.-X. Zhang, Z. Xi, *J. Am. Chem. Soc.* **2017**, *139*, 5039–5042; l) D. Chen, Y. Hua, H. Xia, *Chem. Rev.* **2020**, *120*, 12994–13086; m) S. Gupta, S. Su, Y. Zhang, P. Liu, D. J. Wink, D. Lee, *J. Am. Chem. Soc.* **2021**, *143*, 7490–7500.
- [3] S. Chen, L. Peng, Y. Liu, X. Gao, Y. Zhang, C. Tang, Z. Zhai, L. Yang, W. Wu, X. He, L. L. Liu, F. He, H. Xia, *Proc. Natl. Acad. Sci. USA* **2022**, *119*, e2203701119.
- [4] N. Lu, Z. Deng, J. Gao, C. Liang, H. Xia, P. Zhang, *Nat. Commun.* **2022**, *13*, 2245.
- [5] J. Wang, J. Li, Y. Zhou, C. Yu, Y. Hua, Y. Yu, R. Li, X. Lin, R. Chen, H. Wu, H. Xia, H.-L. Wang, *J. Am. Chem. Soc.* **2021**, *143*, 7759–7768.
- [6] C. Zhu, C. Yang, Y. Wang, G. Lin, Y. Yang, X. Wang, J. Zhu, X. Chen, X. Lu, G. Liu, H. Xia, *Sci. Adv.* **2016**, *2*, e1601031.
- [7] Y. Zhang, S. Zhang, Z. Zhang, L. Ji, J. Zhang, Q. Wang, T. Guo, S. Ni, R. Cai, X. Mu, W. Long, H. Wang, *Front. Chem.* **2021**, *9*, 728066.
- [8] H. Lin, S. Gao, C. Dai, Y. Chen, J. Shi, *J. Am. Chem. Soc.* **2017**, *139*, 16235–16247.
- [9] B. Guo, Z. Sheng, D. Hu, C. Liu, H. Zheng, B. Liu, *Adv. Mater.* **2018**, *30*, 1802591.
- [10] Z. Mi, P. Yang, R. Wang, J. Unruangsri, W. Yang, C. Wang, J. Guo, *J. Am. Chem. Soc.* **2019**, *141*, 14433–14442.
- [11] S. Li, Q. Deng, Y. Zhang, X. Li, G. Wen, X. Cui, Y. Wan, Y. Huang, J. Chen, Z. Liu, L. Wang, C.-S. Lee, *Adv. Mater.* **2020**, *32*, 2001146.
- [12] a) C. Beemelmans, H. U. Reissig, *Chem. Soc. Rev.* **2011**, *40*, 2199–2210; b) R. D. Hancock, *Chem. Soc. Rev.* **2013**, *42*, 1500–1524; c) S. Cao, Z. Ye, Y. Chen, Y.-M. Lin, J. Fang, Y. Wang, B. Yang, L. Gong, *CCS Chem.* **2021**, *3*, 3329–3340.
- [13] a) Y. Ruiz-Morales, *J. Phys. Chem. A* **2002**, *106*, 11283–11308; b) M. Winkler, K. N. Houk, *J. Am. Chem. Soc.* **2007**, *129*, 1805–1815.
- [14] a) Z. Zeng, H. Jin, K. Sekine, M. Rudolph, F. Rominger, A. S. K. Hashmi, *Angew. Chem. Int. Ed.* **2018**, *57*, 6935–6939; *Angew. Chem.* **2018**, *130*, 7051–7056; b) F. Stuck, M. C. Dietl, M. Meissner, F. Sebastian, M. Rudolph, F. Rominger, P. Kramer, A. S. K. Hashmi, *Angew. Chem. Int. Ed.* **2022**, *61*, e202114277; *Angew. Chem.* **2022**, *134*, e202114277.
- [15] Y. Gao, S. Yang, M. She, J. Nie, Y. Huo, Q. Chen, X. Li, X.-Q. Hu, *Chem. Sci.* **2022**, *13*, 2105–2114.
- [16] L. Li, T.-D. Tan, Y.-Q. Zhang, X. Liu, L.-W. Ye, *Org. Biomol. Chem.* **2017**, *15*, 8483–8492.
- [17] Deposition numbers 2192003 (**3c**), 2192014 (**3g**), 2192006 (**3h**), 2192016 (**3j**), 2192015 (**3k**), 2193177 (**4a**), 2193201 (**5a**) contain the supplementary crystallographic data for this paper. These data are provided free of charge by the joint Cambridge Crystallographic Data Centre and Fachinformationszentrum Karlsruhe Access Structures service.
- [18] X. Zhou, X. Pang, L. Nie, C. Zhu, K. Zhuo, Q. Zhuo, Z. Chen, G. Liu, H. Zhang, Z. Lin, H. Xia, *Nat. Commun.* **2019**, *10*, 1488.
- [19] M. Luo, Y. Hua, K. Zhuo, L. Long, X. Lin, Z. Deng, Z. Lin, H. Zhang, D. Chen, H. Xia, *CCS Chem.* **2021**, *3*, 758–763.
- [20] B. Liu, H. Wang, H. Xie, B. Zeng, J. Chen, J. Tao, T. B. Wen, Z. Cao, H. Xia, *Angew. Chem. Int. Ed.* **2009**, *48*, 5430–5434; *Angew. Chem.* **2009**, *121*, 5538–5542.
- [21] M. Luo, Y. Sui, X. Lin, C. Zhu, Z. Yan, Y. Ruan, H. Zhang, H. Xia, *Chem. Commun.* **2020**, *56*, 6806–6809.
- [22] T. Wang, H. Zhang, F. Han, R. Lin, Z. Lin, H. Xia, *Angew. Chem. Int. Ed.* **2012**, *51*, 9838–9841; *Angew. Chem.* **2012**, *124*, 9976–9979.
- [23] a) C. M. Angelov, D. M. Mondeshka, T. N. Tancheva, *J. Chem. Soc. Chem. Commun.* **1985**, 647–648; b) D. Zhao, J. Zhang, Z. Xie, *J. Am. Chem. Soc.* **2015**, *137*, 13938–13942; c) Y. Aida, Y. Shibata, K. Tanaka, *Chem. Asian J.* **2019**, *14*, 1823–1829; d) Y.-F. Lv, F.-C. Ren, M.-T. Kuang, Y. Miao, Z.-L. Li, J.-M. Hu, J. Zhou, *Org. Lett.* **2020**, *22*, 6822–6826; e) Q. Feng, A. Wu, X. Zhang, L. Song, J. Sun, *Chem. Sci.* **2021**, *12*, 7953–7957.
- [24] a) A. Fujiya, M. Tanaka, E. Yamaguchi, N. Tada, A. Itoh, *J. Org. Chem.* **2016**, *81*, 7262–7270; b) K. Mullick, S. Biswas, A. M. Angeles-Boza, S. L. Suib, *Chem. Commun.* **2017**, *53*, 2256–2259; c) M.-M. Xun, Y. Bai, Y. Wang, Z. Hu, K. Fu, W. Ma, C. Yuan, *Org. Lett.* **2019**, *21*, 6879–6883; d) D.-H. Liu, H.-L. He, Y.-B. Zhang, Z. Li, *ACS Sustainable Chem. Eng.* **2020**, *8*, 14322–14329.
- [25] C. Zhu, X. Zhou, H. Xing, K. An, J. Zhu, H. Xia, *Angew. Chem. Int. Ed.* **2015**, *54*, 3102–3106; *Angew. Chem.* **2015**, *127*, 3145–3149.
- [26] a) H. Jin, L. Huang, J. Xie, M. Rudolph, F. Rominger, A. S. K. Hashmi, *Angew. Chem. Int. Ed.* **2016**, *55*, 794–797; *Angew. Chem.* **2016**, *128*, 804–808; b) S. Kim, S. H. Han, N. K. Mishra, R. Chun, Y. H. Jung, H. S. Kim, J. S. Park, I. S. Kim, *Org. Lett.* **2018**, *20*, 4010–4014; c) M. H. Tsai, C. Y. Wang, A. S. Kulan-dai Raj, R.-S. Liu, *Chem. Commun.* **2018**, *54*, 10866–10869; d) J. Li, E. Tan, N. Keller, Y.-H. Chen, P. M. Zehetmaier, A. C. Jakowetz, T. Bein, P. Knochel, *J. Am. Chem. Soc.* **2019**, *141*, 98–103; e) Y.-C. Hsu, S.-A. Hsieh, R.-S. Liu, *Chem. Eur. J.* **2019**, *25*, 5288–5297; f) X. Tian, L. Song, K. Farshadfar, M. Rudolph, F. Rominger, T. Oeser, A. Ariafard, A. S. K. Hashmi, *Angew. Chem. Int. Ed.* **2020**, *59*, 471–478; *Angew. Chem.* **2020**, *132*, 479–486; g) P. E. Simm, P. Sekar, J. Richardson, P. W. Davies, *ACS Catal.* **2021**, *11*, 6357–6362.
- [27] S.-Y. Zhuang, Y.-X. Tang, C. He, X.-L. Chen, W.-J. Xue, Y.-D. Wu, A.-X. Wu, *Adv. Synth. Catal.* **2021**, *363*, 1137–1141.
- [28] C. Yang, G. Lin, C. Zhu, X. Pang, Y. Zhang, X. Wang, X. Li, B. Wang, H. Xia, G. Liu, *J. Mater. Chem. B* **2018**, *6*, 2528–2535.
- [29] A. Wadsworth, M. Moser, A. Marks, M. S. Little, N. Gasparini, C. J. Brabec, D. Baran, I. McCulloch, *Chem. Soc. Rev.* **2019**, *48*, 1596–1625.

Manuscript received: August 9, 2022

Accepted manuscript online: October 3, 2022

Version of record online: October 25, 2022